7th Asia-Pacific Workshop on Structural Health Monitoring
November 12-15, 2018 Hong Kong SAR, P.R. China

Experimental modal analysis of Rod-fastening Rotor under different Pre-tension forces

Zhou Chuandi[1], Liu Yibing[1], Zhao Li[1,2], Hu Liang[3], Teng Wei[1]*, Zhang Chunjian[1]

[1] Key Laboratory of Condition Monitoring and Control for Power Plant Equipment, Ministry of Education, North China Electric Power University, Beijing, China
Email: zcd@ncepu.edu.cn; lyb@ncepu.edu.cn; tengw@ncepu.edu.cn;

[2] SPIC Tianjin Branch, Tianjin, China

[3] China University of Mining and Technology, Beijing, China

KEYWORDS: Rod-fastening rotor; Modal test; LSCE; Tension force;

ABSTRACT

Gas turbines are widely used in power generation. The rotor structure of a gas turbine is normally multi-disc Rod-fastening one, that is different from that of a steam turbine rotor. Rod tension forces of a rotor are very important for safety running of the gas turbine. In order to monitor the health condition of a rod-fastening Rotor, a group of modal tests on a multi-disc rod-fastening rotor were conducted under different rod preloads, the modal parameters of the rotor are identified from measurement data by means of LSCE methods. Test results show that first two natural frequency of the rod-fastening rotor increases with the increase of the rod pre-tightening force.

1. Introduction

Gas turbine power generation is a clean power generation technology that has received widespread attention in recent years. Compared with conventional steam generators, gas turbine generators have higher integration and more complex structures. The rod-fastening rotor is assembled through multiple axially stretched pull rods to tighten the discs. Therefore, the tension force relaxation of the pull rods may occur during long-term operation, which has an effect on the inherent characteristics and dynamic characteristics of the rod-fastening rotor.

Theoretically, tension force of the rod fastening rotor is an important parameter that affects the contact stiffness of the discs and dynamic characteristics of the rod-fastening rotor. Thus, the influence of the tension force of the rod-fastening rotor on the contact stiffness has been concerned by many scholars. The researchers have established theoretical models of the contact stiffness of discs and discussed the influence on the dynamic characteristics of the rotor. Rao Zhushi et al. [1-3] proposed a theoretical calculation method for rough surface contact stiffness and conducted a rod fastening rotor mechanics model by using elastic contact theory and probabilistic analysis methods. Wang Ailun et al. [4-6] established a coupling dynamics bond diagram model of a multiple disc rod-fastening rotor and studied the bending, axial and torsional vibrations of the rotor by considering the contact effect on the discontinuous interface. Gao Jin et al. [7] considered the contact between the discs as a torsion spring to analyse the torsional vibration of a rod-fastening rotor. Wang Shaobo et al. [8] established a rotor-

* Teng Wei

support system dynamic model based on the Riccati transfer matrix method and calculated the critical speed and mode shapes of the rotor. In addition, finite element model of rod-fastening rotors were established in literatures [9-12], and the finite element analysis were performed to obtain the natural frequency, critical speed and mode shapes of the rotor. What's more, many scholars [13-17] considered the contact effect between the discs, established nonlinear dynamic models of rod fastening rotors and conducted nonlinear dynamics research. Through theoretical research, it is found that the contact stiffness between the rotor discs increases with the increase of tension force of the rods, which makes the rod-fastening rotor closer to the integral rotor. Thus, the natural frequencies of the rod fastening rotor also increase.

Although many scholars have conducted a lot of theoretical studies, there have been few experimental studies on the effect of tension force on the inherent characteristics of the rod-fastening rotor. The literature [18] carried out a rotation experiment of a rod-fastening rotor and studied the influence of the tension force of the rod on the critical rotation speeds. The literature [19] carried out a modal test experiment on a rod-fastening rotor model at free state and studied the influence of the normal load on the natural frequency of the bending vibration.

In this paper, the experimental study on the dynamic characteristics of a rod-fastening rotor under different pre-tension forces was carried out. The modal parameters of rod fastening rotor under different pre-tension forces were tested and analysed by the hammering and LSCE method. The experiment results provide a certain basis for theoretical research.

2. Experimental modal analysis

2.1 Modal information acquisition

For a multi-degree-of-freedom structural damping system, the basic vibration equation is:

$$[M]\{\ddot{x}(t)\}+[C]\{\dot{x}(t)\}+[K]\{x(t)\}=\{f(t)\} \tag{1}$$

Where *[M]* is the mass matrix, *[K]* is the stiffness matrix, *[C]* is the damping matrix, *{[x(t)]}* is the displacement vector, and {f(t)} is the excitation vector.

Make the excitation be $\{f(t)\}=\{F\}e^{j\omega t}$ and the displacement be $\{x(t)\}=\{X\}e^{j\omega t}$, function (1) can be write as

$$\left(-\omega^2[M]+j\omega[C]+[K]\right)\{X\}=\{F\} \tag{2}$$

Without considering damping, Equation (2) becomes

$$\left(-\omega^2[M]+[K]\right)\{X\}=\{F\} \tag{3}$$

When considering $F=0$, Equation (3) becomes

$$\left|-\omega^2[M]+[K]\right|=0 \tag{4}$$

Then n eigenvalues (r=1, 2, ... n) can be obtained. The square root ω_r is the natural frequency of the system and it satisfies

$$\left(-\omega^2[M]+[K]\right)\{\varphi_r\}=0 \tag{5}$$

Where $\{\varphi_r\}\left(r=1,2,\cdots,n\right)$ is the modal vector of the system and it can be used to identify the mode shapes.

If equation (2) is written in a matrix,

$$\{X\}=\sum_{r=1}^{n}\frac{\{\varphi_r\}\{\varphi_r\}^T}{-\omega^2 M_r+j\omega C_r+K_r}\{F\}$$

$$=\begin{bmatrix} H_{11} & H_{12} & \cdots & H_{1m} \\ H_{21} & H_{22} & \cdots & H_{2m} \\ \vdots & \vdots & \vdots & \vdots \\ H_{m1} & H_{m2} & \cdots & H_{mm} \end{bmatrix}\begin{bmatrix} F_1 \\ F_2 \\ F_3 \\ F_4 \end{bmatrix} \tag{6}$$

Any row in the frequency response function matrix is

$$\begin{bmatrix} H_{i1} & H_{i2} & \cdots & H_{iN} \end{bmatrix}=\sum_{r=1}^{N}\frac{\varphi_{ir}}{-\omega^2 M_r+j\omega C_r+K_r}[\varphi_{1r} \quad \varphi_{2r} \quad \cdots \quad \varphi_{Nr}] \tag{7}$$

Any column in the frequency response function is

$$\begin{Bmatrix} H_{1j} \\ H_{2j} \\ \vdots \\ H_{Nj} \end{Bmatrix}=\sum_{r=1}^{N}\frac{\varphi_{jr}}{-\omega^2 M_r+j\omega C_r+K_r}\begin{Bmatrix} \varphi_{1r} \\ \varphi_{2r} \\ \vdots \\ \varphi_{jr} \end{Bmatrix} \tag{8}$$

That is, any row or column in the frequency response function contains all the modal parameters. The ratio of frequency response function of the r-th mode of the row or the column is the r-th mode shape.

For the hammer test, if the hammer is moved and the sensor is fixed, one row in the frequency response function can be obtained. If the hammer is fixed and the sensor is moved, one column of the frequency response functions can be obtained. As shown in Figure 1, the hammer is fixed, and the sensor is moved to measure the transfer function between each measuring point and the impact point. Then a column of elements in the entire structure transfer function matrix can be obtained. Therefore, the complete modal information of the structure is obtained.

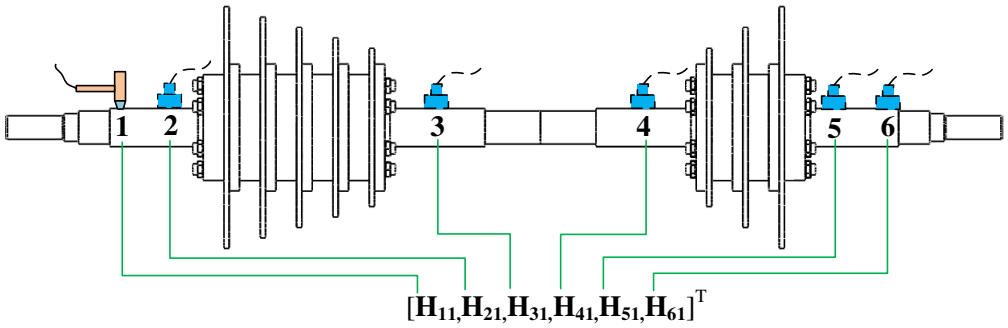

Figure 1. Hammering method to obtain frequency response function

2.2 Time Domain Multiple Reference Point Algorithm

Time domain multi-reference point algorithm, also known as multi-reference point least square complex index method (LSCE), is a commonly used method to estimate modal parameters.

For a multi-degree-of-freedom viscous-damping linear system, the frequency response function for the point p caused by the q is

$$H_{pq}(j\omega) = -\sum_{r}^{N}\left[\frac{A_{rpq}}{j\omega - s_r} + \frac{A_{rpq}^{*}}{j\omega - s_r^{*}}\right] \tag{9}$$

Where: A_{rpq} is the residue of the r-th mode; N is the number of degrees of freedom of the system; s_r is the pole of the frequency response function of the r-th mode, which is related to the modal frequency and damping.

The pole s_r is given by:

$$s_r = -\omega_r\zeta_r + j\omega_r\sqrt{1-\xi_r^2} \tag{10}$$

where ω_r is the natural frequency of the system and ξ_r is the damping ratio.

If the measured impulse response function is a discrete time series with the intervals of Δt, then at $t_k=k\Delta t$, the impulse response function can be expressed as:

$$h_k = h(k\Delta t) = \sum_{r=1}^{2N} A_r e^{s_r t_k} = \sum_{r=1}^{2N} A_r e^{s_r k\Delta t} = \sum_{r=1}^{2N} A_r V_r^k \quad (\text{k=0,1,2,…L}) \tag{11}$$

Where $V_r = e^{s_r t_k}$, $L+1$ is the data length of the impulse response function of the measured signal, and $L+1$ is much larger than $2N$.

For equation (11), V_r are the roots of a $2N$ polynomial equation with real coefficients (natural regression coefficients) given by

$$\sum_{r=1}^{2N} \beta_{\mathrm{k}} V^k = \prod_{r=1}^{N}(V - V_k)(V - V_k^{*}) = 0 \tag{12}$$

Obviously, $\beta_{2N}=1$. Multiplying each equation (11) by the corresponding β_k, equation (13) is obtained:

$$\sum_{r=1}^{2N} \beta_{\mathrm{k}} h_k = \sum_{r=1}^{2N} \beta_{\mathrm{k}} \sum_{r=1}^{2N} A_r V_r^k = \sum_{r=1}^{2N} A_r \sum_{r=1}^{2N} \beta_{\mathrm{k}} V_r^k \tag{13}$$

For each V_r, $\sum_{r=1}^{2N} \beta_{\mathrm{k}} V_r^k = 0$, $\beta_{2N} = 1$, equation (12) can be simplified as

$$\sum_{k=1}^{2N-1} \beta_{\mathrm{k}} h_k = -h_{2N} \tag{14}$$

Equation (14) can be used to estimate the autoregression coefficient β_k. Taking $2N+1$ data from the actual measurement h_k and carrying it into equation (14) by shifting Δt backwards at each sampling time, the following is obtained:

$$\begin{bmatrix} h_0 & h_1 & h_2 & \cdots & h_{2N-1} \\ h_1 & h_2 & h_3 & \cdots & h_{2N} \\ \vdots & \vdots & \vdots & & \vdots \\ h_{M-1} & h_M & h_{M+1} & \cdots & h_{L-1} \end{bmatrix} \begin{bmatrix} \beta_0 \\ \beta_1 \\ \vdots \\ \beta_{2N-1} \end{bmatrix} = - \begin{bmatrix} h_{2N} \\ h_{2N+1} \\ \vdots \\ h_L \end{bmatrix} \tag{15}$$

which can be written as

$$[h]\beta = -[h^{'}] \tag{16}$$

Use the pseudo-inverse method to find the least-squares solution of equation (16):

$$\{\beta\} = ([h]^T[h])^{-1}([h]\{h^{'}\}) \tag{17}$$

The $\beta_{2N}=1$ then is added into $\{\beta\}$ to obtain the root V_r of the polynomial consisting of the coefficient β_k in equation (12). Then the modal frequency ω_r, and the damping ratio ξ_r can be calculated by:

$$\omega_r = \frac{1}{\Delta t}\sqrt{\ln V_r \ln V_r^*} \qquad \xi_r = -\frac{\ln(V_r V_r^*)}{2\omega_r \Delta t} \tag{18}$$

3. Modal experiment of rod-fastening rotor

3.1 Description of experimental subjects

The structure of the rod-fastening rotor is shown in figure 2. The whole structure includes of a base, a driving motor, a rotor of a simulated compressor, a coupling, a turbine rotor, and a permanent magnet generator. The rotor, about 2 meters in length, is divided into two rotors with discs connected by rigid couplings. In the figure, the left part of the rotor consists of 5 discs, which are used to simulate the rotor part of the compressor. The right part of the rotor consists of 3 discs, which are used to simulate the turbine rotor. Both parts of the discs are tightened by 6 circumferential rods. One end of the rotor is connected with a drive motor, and the other end is equipped with a generator as the load, which can realize grid-connected power generation.

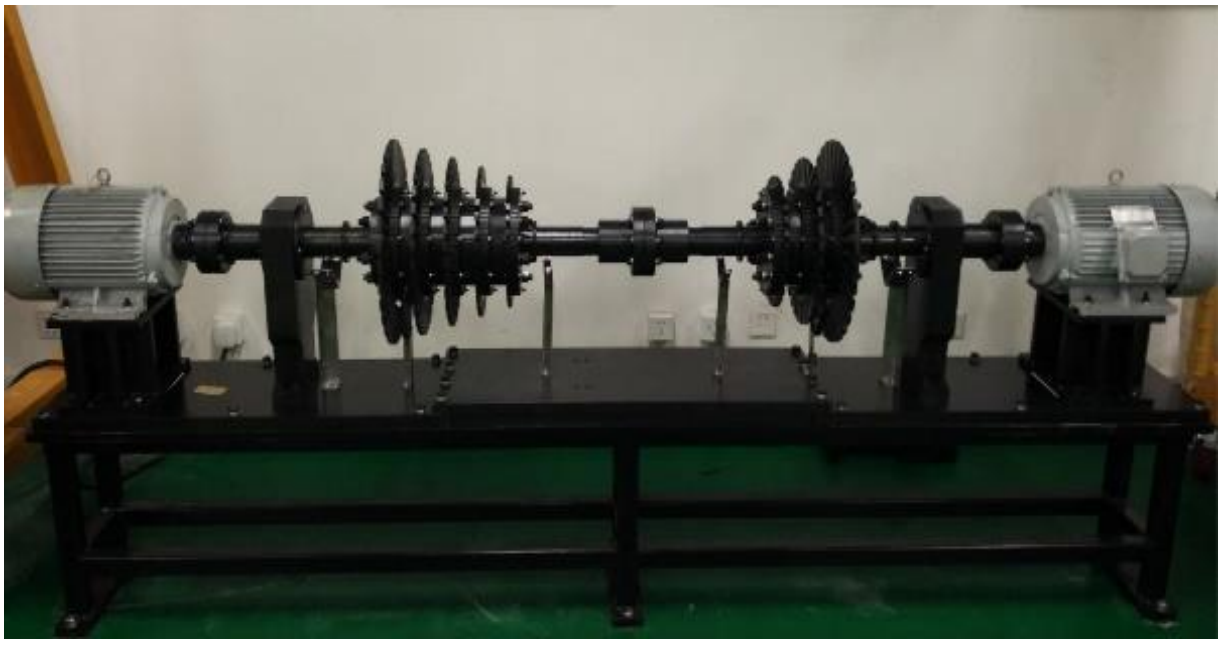

Figure 2. The structure of rod-fastening rotor

3.2 Instrument and test points layout

The modal test instrument is the vibplot modal test system produced by m+p company of Germany. The signal acquisition front-end device is m+p vibRunner 16-channel LXI bus, which can collect up to 16 channel signals at the same time. The signal analysis software is SmartOffice V4.4, which can carry out signal processing and extract modal information. Table 1 shows the main parameters of the test instrument.

Table 1. Technical parameters of modal test instruments

Number	Device name	Specifications	Technical indicators
1	Force hammer	086C41	Charge type; Maximum excitation force 40000N
2	Acceleration sensor	PCB3097A2	Frequency response：0.3-100Hz
3	Data acquisition front end	m+p vibpilot-8	16 channels
4	Signal analysis software	m+p SmartOfficeV4.3	Modal parameter extraction

The frequency response function was obtained through the hammering method by fixing force hammer and moving sensors. In the experiment, 5 points were set along the axial direction and each point was arranged an acceleration sensor to collect the response signal. Since we focused mainly on the bending vibration of the rotor and considering the rotor structure of symmetry, the rod fastening rotor model was simplified to a long pole to represent the testing model. The length of the model and the measuring points layout are shown in figure 3. In the process of pre-experiment, it was found that the support stiffness at point 3 was good and the incentive transfer performance was strong. Therefore, point 3 was selected as the excitation point of modal test. In the test, the direction of excitation applied by the force hammer was Z direction, and the acceleration signal collected by the sensor was also Z direction.

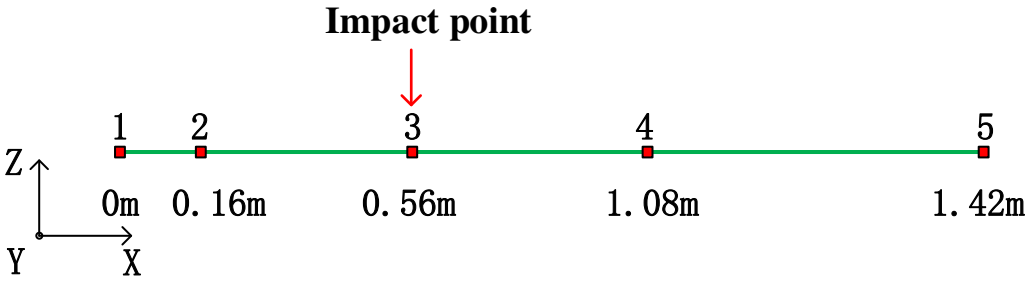

Figure 3. Simplified model of the rotor for modal test

3.3 Experimental content

The experimental process are as follows:

(1) adjust the pre-tension force of the pull rods;

(2) rotate the rotor to a fixed position;

(3) perform hammer test, and collect the rotor excitation response signal;

(4) analyze the measurement data and extract the modal parameters (natural frequency, damping and mode shapes) of the rod fastening rotor.

The tension bolt used in the test is M16 in specification whose strength class is 6.8. The ultimate torque is 137N·m. According to the empirical formula between the pre-tension force of thread and the tightening torque given in literature [20], the pre-tension force of each pull rod can be calculated.

The empirical formula is

$$F = \frac{T}{KD} \tag{19}$$

Where, F is the tension force, T is the tightening torque, D is the nominal diameter of the thread, K is the thread coefficient (usually is 0.2).

In the experiment, the tightening torque of the rotor was set as 20 N·m, 30 N·m, 40 N·m, 50 N·m, 60 N·m, 70 N·m, 80 N·m, 90 N·m and 100 N·m, and hammer test was conducted in each state successively. The tension forces of the corresponding pull rods under different torques are shown in Table 2.

Table 2. Tension of the pull rods under different torques

Torque(N·m)	20	30	40	50	60	70	80	90	100
Tension force(N)	6250	9375	12500	15625	18750	21875	25000	28125	31250

During the test, the pull rods were twisted to the relaxed state, and then the torque wrench was used for the pre-tightening operation. In order to ensure the balance of the pre-tightening forces, a circumferential symmetric cross pre-tightening method was adopted to pre-tighten the pull rods. The pre-tightening sequence is shown in Figure 4. After pre-tightening, the modal test under this tension state was carried out by hitting the excitation point. Then recording the excitation signal of the hammer and the response signal of each response point. During the test, the mean value of three hammering was measured to ensure the accuracy of the experiment.

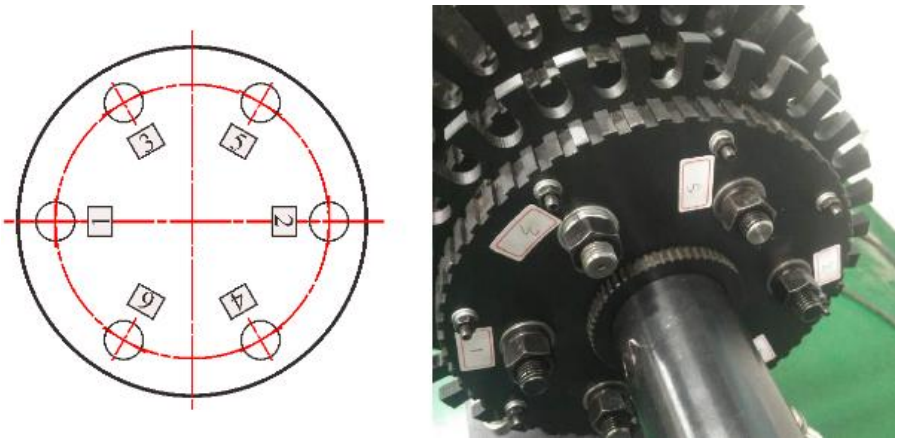

Figure 4. Pre-tightening sequence of the pull rods

4. Analysis of results

Based on the excitation and response test data, the dynamic flexibility matrix of the rotor structure is calculated, and the modal parameters are identified based on time domain multiple reference point algorithm. Figure 5 shows a set of test analysis results such as excitation signal, response signal, frequency response function, and coherence function under the pre-tightening torque of 50 N·m. The signal acquisition time is 3 s. As can be seen from the figure, the excitation signal of the hammer is an

instantaneous impact, and the response signals of the measurement points are oscillation attenuation signals. Taking the excitation signal as the input and the response signal as the output, the frequency response function curve can be calculated as shown in Figure 5.c. The obvious peaks indicate that the structure is excited by the force hammer and the amplitude reaches the maximum at the resonance frequency. The coherence functions shown in Figure 5.d are greater than 0.8 between the analysis frequency range (20-120 Hz). Based on engineering experience, it can be considered that the coherence of the excitation signals and the response signals are good, which shows high reliability of the experimental results.

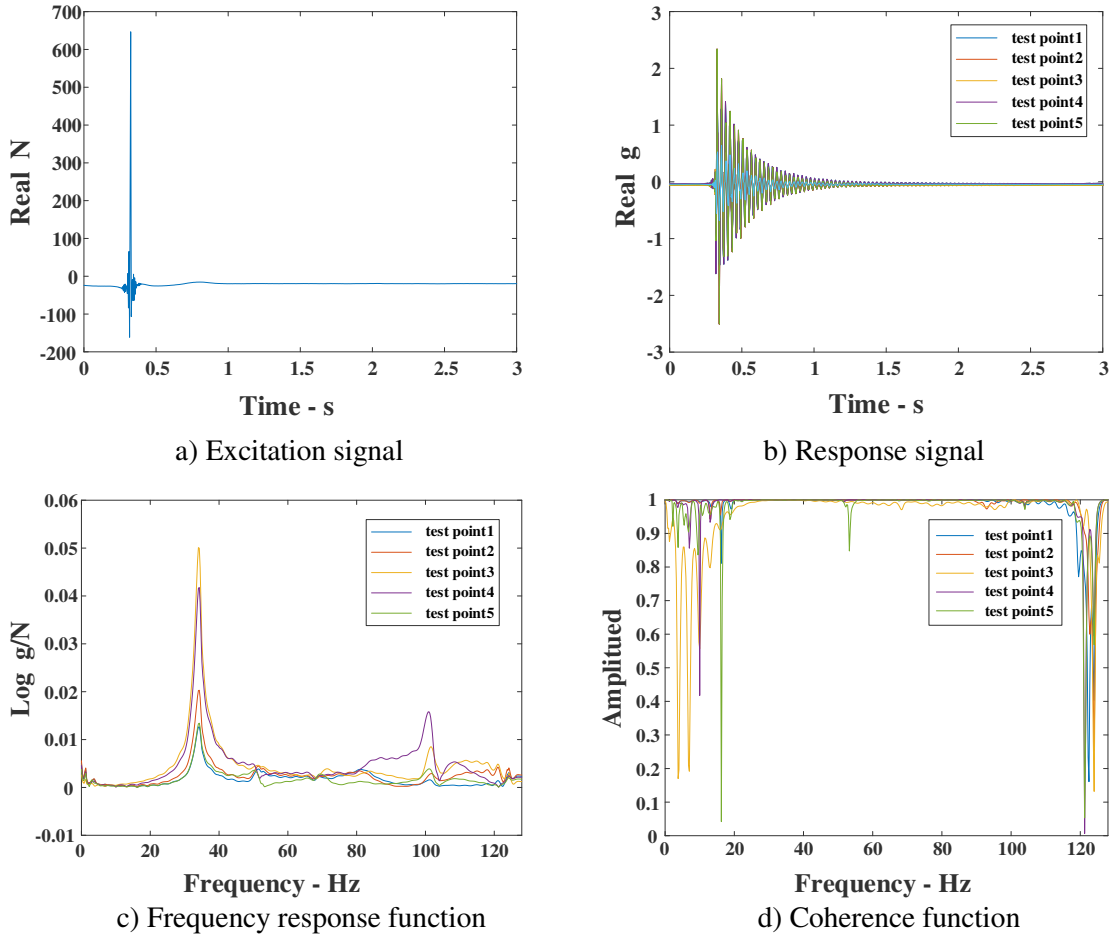

a) Excitation signal b) Response signal

c) Frequency response function d) Coherence function

Figure 5. Test data of the experiment

Figure 6 is the system pole diagram and stability diagram. The frequency response curves and calculated poles are shown in the diagram. The selected frequency range is 0 - 120 Hz when obtain the stability diagram, and the calculated modal orders are second orders. The points represented by rhombic blocks in the figure represent the poles with stable frequency, damping and participation factors. The results show that the system has stable poles under two obvious peaks. One stable pole at the first peak is between 30 and 40 Hz, and the other stable pole at the second peak is between 100 and 106 Hz.

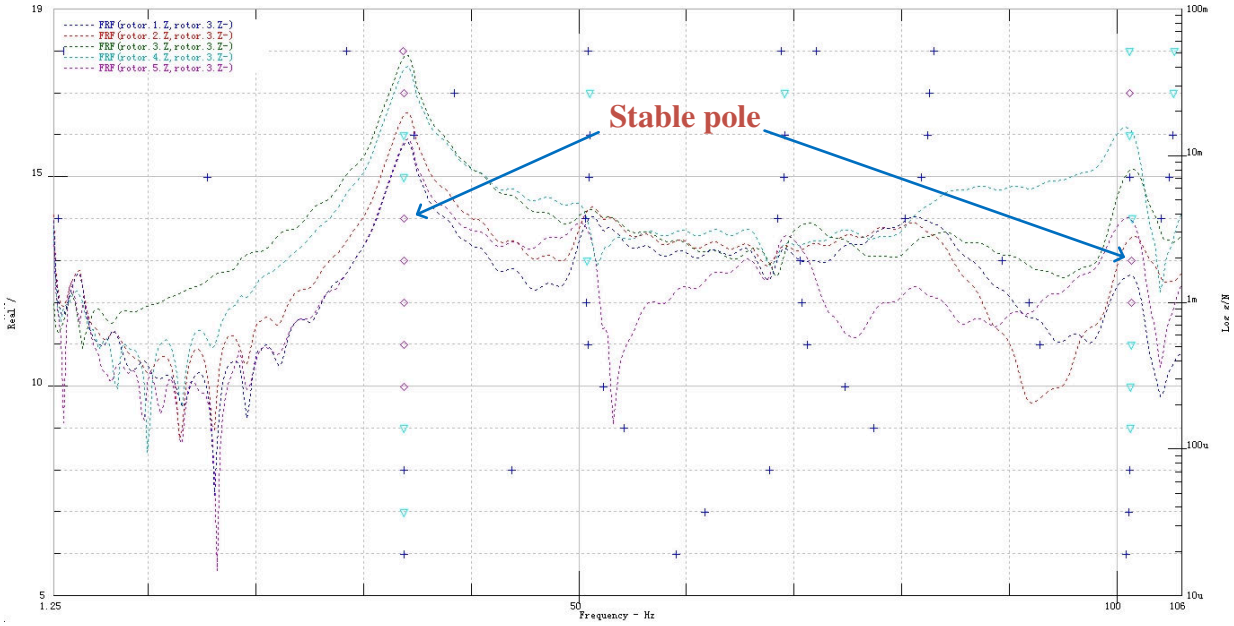

Figure 6. System pole diagram and stability diagram

By fitting the frequency response function curve, the FRF curve of excitation point is obtained as shown in Figure 7. From the amplitude and phase curves, it can be seen that the phase changes abruptly at two peaks of the frequency response function curve. In the real imaginary part graph, the imaginary part of the curve generates the extreme value at the peak of the real part curve. Therefore, it can be concluded that the frequencies corresponding to the two peaks of the frequency response function are the natural frequencies of the rod fastening rotor. The first two natural frequencies and damping values of the rotor under the pre-tightening torque of 50 N·m are shown in Table 3. The first natural frequency of rotor is 33.83 Hz with the damping ratio 2.30 %, and the modal shape is bending vibration in Z direction. The second-order natural frequency is 100.57 Hz with the damping ratio 2.12 %, and the modal shape is bending vibration in Z direction.

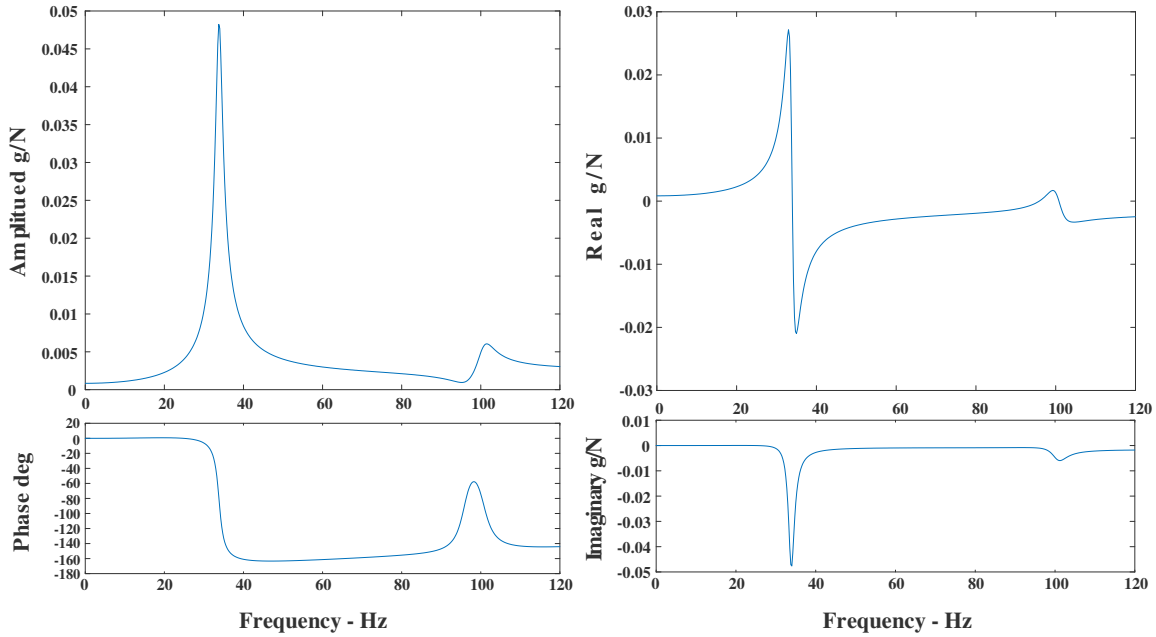

a) Amplitude and phase characteristic b) Real and imaginary characteristics

Figure 7. Fitting curve of frequency response function

Table 3. First 2 modal parameters of the rotor

Order number	Natural frequency（Hz）	Damping ratio（%）	Mode description
1	33.83	2.30	first order bending vibration
2	100.57	2.12	Second order bending vibration

The frequency response function curves of the excitation point under all tightening torque states are shown in Figure 8. It can be seen that with the increase of tension force of rod, the positions of two peaks of frequency response function gradually shift, which indicates that the natural frequency of the rotor are gradually changing. The natural frequency values under different tightening torques are listed in Table 4. The data shows that the natural frequency of the rotor gradually increases with the increase of tension force. In the range of experimental pre-tightening force, the first-order natural frequency of rod fastening rotor increased by 1.3 Hz and the second-order natural frequency increased by 1.57 Hz. If the natural frequency is converted into the critical speed, the first-order critical speed of the rotor increased by 78 n / min, and the second-order critical speed increased by 94.2 n / min.

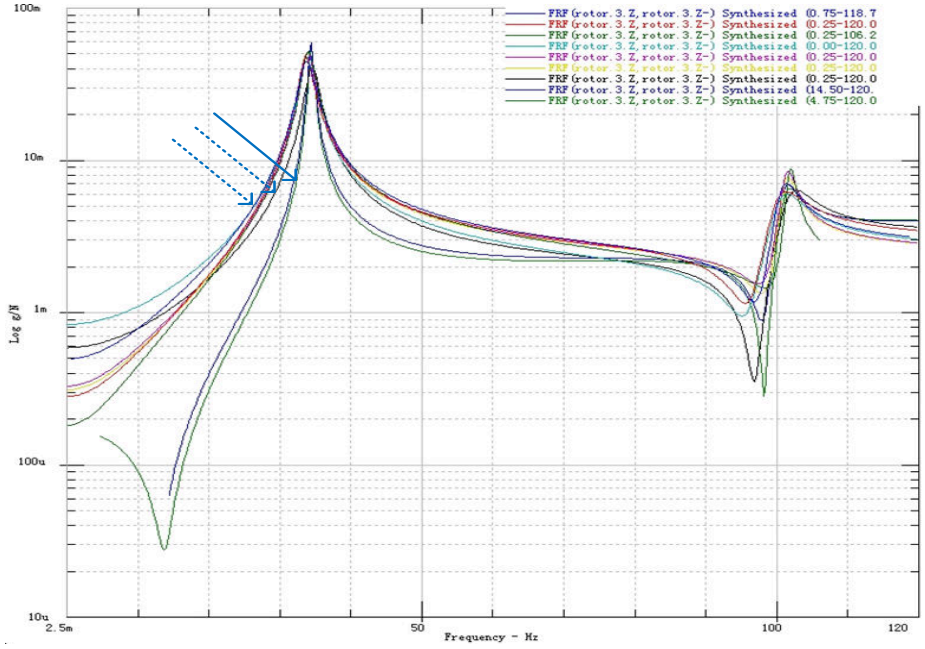

Figure 8. Fitting curves of FRF under different pre-tightening forces.

Table 4. Natural frequencies of the rotor under different tension forces.

Torque（N·m）	20	30	40	50	60	70	80	90	100
Tension force（N）	6250	9375	12500	15625	18750	21875	25000	28125	31250
First-order natural frequency（Hz）	33.38	33.51	33.68	33.83	33.97	33.99	34.64	34.66	34.68
Second-order natural frequency（Hz）	100.21	100.34	100.51	100.57	101.37	101.39	101.73	101.74	101.78

To show the relationship between the natural frequency and the tightening torque more clearly, polynomial regression method is adopted to fit the data in Table 4, and the fitting curves between the

tightening torque and the natural frequency are shown in Figure 9. The results indicate that with the increase of tightening torque, the first two natural frequencies of the rotor are increasing.

From the fitting curves in the figure, it can be seen that when the torque is less than 80 N·m, the second-order natural frequency of the rotor increases faster than the first-order natural frequency, which indicates that the second-order natural frequency of the rotor is more sensitive to the change of tension force when the torque is small. When the torque is greater than 80 N·m, the growth rate of the first-order natural frequency of the rotor has not changed significantly, and the growth rate of the second-order natural frequency has slowed down with a smaller range of change.

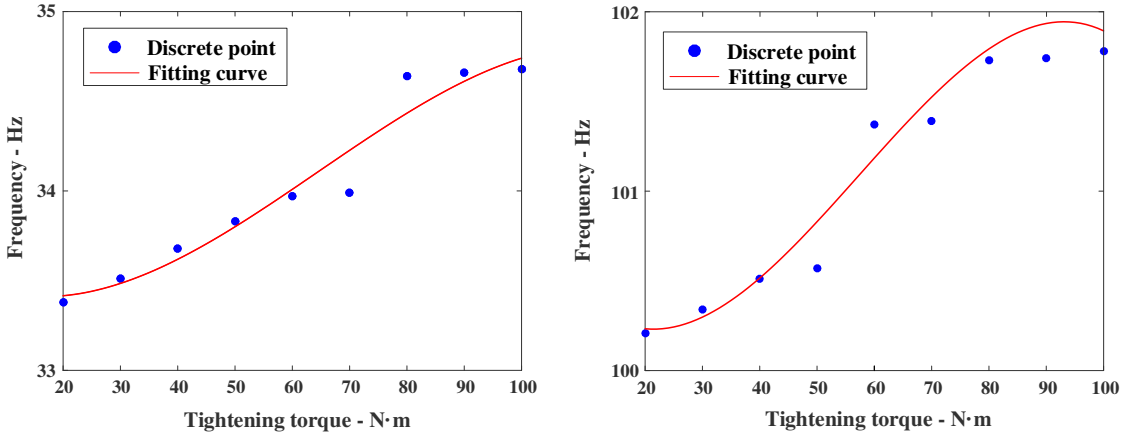

a) The first-order natural frequency b) The second-order natural frequency

Figure 9. Fitting curve of natural frequency with tightening torque

5. Conclusion

The experimental model of rod-fastening rotor was tested by hammering method, and the modal experiments of rod-fastening rotor under different tension forces were carried out. The steady-state diagram of frequency response function was obtained by using time domain multi-reference point algorithm, and the first two natural frequencies and dampings of the rotor were extracted. The results show that under different pretensions, the first-order natural frequency range is 33 - 35 Hz, and the second-order natural frequency range is 100 - 102 Hz.

The curve of the natural frequency of the rod-fastening rotor with the change of tightening torque is obtained. The experimental results indicate that with the increase of pre-tension force, the natural frequency of the rotor tends to increase. When the tightening torque is small, the second-order natural frequency of the rotor increases faster than the first-order frequency. When the pre-tightening force increases to a certain degree, the growth rate of the first-order natural frequency does not obviously change, and the growth rate of the second-order natural frequency slows down.

From the experimental results, it can be concluded that the tension force of the rods has an influence on the natural frequency of the rotor. The regulation that the natural frequency of the rotor gradually increases with the increase of the tension force is consistent with the theoretical research. However, the change of actual contact stiffness between discs caused by tension in theoretical research can't be given in this experiment, which requires further experimental research.

Acknowledgement

This work is supported by the Research Funds for the Central Universities Achievement Transformation in Beijing (No. ZDZH20141005401)

References and Footnotes

[1] Rao Zhushi, Xia Songbo, Wang Guangming, A Study Of Contact Stiffness Of Flat Rouge Surfaces[J]. Journal of Mechanical Strength, 1994, 16(02): 71-75.

[2] Wang Guangming et al. The Analysis Of Mechanical Model Of Rod Fastening Rotor [J]. Journal of Acta Aeronautica ET Astronautica Sinica. 1993, 14(08): 419-423.

[3] Rao Zhushi, Xia Songbo, Wang Guangming, Experimental Study and Computation of a Combined Special Rotor Vibration Mode[J]. Journal of Vibration and Shock, 1996, 15(01): 68-70.

[4] Wang Ailun, Luo Zhou, Research on torsional vibration of tie rod rotor[J]. Journal of Vibration and Shock, 2009. 28(5): 165-168.

[5] Wang Ailun, Research on Rod Fastening Rotor Dynamics—axial Vibration [J]. China Mechanical Engineering, 2009. 20(13): 1524-1527.

[6] Zhang Shengcong, Study on Vibration Characteristics of Disc Tie Rod Rotor[J]. Journal of Vibration and Shock, 2009. 28(4): 117-120.

[7] GAO Jin et al. Torsional Vibration Modal Analysis of Gas Turbine Rod Rotor Considering Contact Effect[J]. Journal of Vibration and Shock, 2012(12): 9-13.

[8] Wang Shaobo, Dynamic Modeling and Critical Speed Calculation of Gas Turbine Rod fastening Rotor[J]. Journal of Shanghai Jiaotong University, 2013. 47(3): 381-391.

[9] Pirogova, N.S. and P.A. Taranenko, Calculative and Experimental Analysis of Natural and Critical Frequencies and Mode Shapes of High-speed Rotor for Micro Gas Turbine Plant. Procedia Engineering[C], 2015. 129: p. 997-1004.

[10] Roy, H. and S. Chandraker, Dynamic study of viscoelastic rotor: Modal analysis of higher order model considering various asymmetries[J]. Mechanism and Machine Theory. 2017, 109: 65-77.

[11] Roy, H., et al., Dynamics of multilayer, multidisc viscoelastic rotor–An operator based higher order classical model[J]. Journal of Sound and Vibration. 2016. 369: 87-108.

[12] Taplak, H. and M. Parlak, Evaluation of gas turbine rotor dynamic analysis using the finite element method[J]. Measurement. 2012, 45(5): 1089-1097.

[13] Li Zhonggang et al. Dynamic characteristics analysis of torsional vibration system of distributed tie rod rotor[J]. Journal of Dynamic and Control,2016, 14(2): 143-146.

[14] Hu Liang et al. Nonlinear Dynamic Response of a Rod Fastening Rotor with a Transverse Crack [J]. NOISE AND VIBRATION CONTROL, 2016, 36(05): 11-14.

[15] Hu Liang, et al. Nonlinear Dynamic Response Characteristics of a Rod Fastening Rotor with Rub-Impact Faults[J]. Journal of Chinese Society of Power Engineering, 2017, 37(07): 533-539.

[16] Di, H., et al., Nonlinear dynamic behaviors of a rod fastening rotor supported by fixed–tilting pad journal bearings[J]. Chaos, Solutions & Fractals, 2014, 69:129-150

[17] Lyantsev, O.D., A.V. Kazantsev and A.I. Abdulnagimov, Identification Method for Nonlinear Dynamic Models of Gas Turbine Engines on Acceleration Mode [J]. Procedia Engineering, 2017, 176:409-415.

[18] He Peng et al., Experiments on the changing law of critical speed of tie rod rotor with tension force[J]. Journal of Vibration, Measurement and Diagnosis, 2014,34(04):644-649+775.

[19] Lu Mingjian,Ruan Haipeng,Xu Guohui,Yan Lie.Analysis and Experimental Research on Dynamic Characteristics and Experimental Investigation of Preloaded Spherical Rotor-bearing Rotor-bearing System[J].Journal of Vibration Engineering,2014,27(01):111-117.

[20] Bickford J.H., An introduction to the design and behavior of bolted joints[M]. Boca Raton: CRC press, 1995.